Evaluation of the Hydrometeor Layers in the East and West Pacific within ISCCP Cloud-Top Pressure–Optical Depth Bins Using Merged *CloudSat* and *CALIPSO* Data

GERALD G. MACE

University of Utah, Salt Lake City, Utah

FORREST J. WRENN

NASA Langley Research Center, Hampton, Virginia

(Manuscript received 5 April 2012, in final form 17 June 2013)

ABSTRACT

The International Satellite Cloud Climatology Project (ISCCP) provides a multidecadal and global description of cloud properties that are often grouped into joint histograms of column visible optical depth τ and effective cloud-top pressure P_{top}. It has not been possible until recently to know the actual distributions of hydrometeor layers within the ISCCP P_{top}–τ bins. Distributions of hydrometeor layers within the ISCCP P_{top}–τ conditional probability space using measurements from the *CloudSat* Cloud Profiling Radar and the *Cloud–Aerosol Lidar and Infrared Pathfinder Satellite Observations* (*CALIPSO*) lidar within two 40° × 40° regions in the eastern and western equatorial Pacific over a 2-yr period are examined. With the exception of thin cirrus and stratocumulus, the authors show that of the P_{top}–τ types that are commonly analyzed, none of the types contain unique distributions of geometrically defined layer types but tend to be populated by diverse sets of hydrometeor layers whose bulk profile properties conspire to render specific radiative signatures when interpreted by two-channel visible and IR sensors from space. In comparing the geometric distribution of cloud layers for common P_{top}–τ types, it is found that the ISCCP Cirrostratus, Deep Convection, and Stratocumulus types appear to have been drawn from a common geometric distribution of hydrometeor layers. The other six common ISCCP P_{top}–τ types do not share this feature. The authors can confidently reject an assumption that even though they have common top-of-atmosphere radiative signatures, they do not appear to share a common distribution of cloud layers and therefore are likely to have significantly different radiative heating profiles and different surface radiative forcing even though their top-of-atmosphere radiative signatures are similar.

1. Introduction

The International Satellite Cloud Climatology Project (ISCCP; Rossow and Schiffer 1999) uses weather satellite observations and global retrievals of the atmospheric thermodynamic state to derive cloud occurrence, the visible column optical depth τ, and the effective cloud-top pressure P_{top}. The ISCCP dataset is global, spans 30 years, and has emerged as a baseline description of cloudiness in Earth's atmosphere (e.g., Rossow and Zhang 1995; Rossow and Zhang 1995; Chen et al. 2000). Additionally, based on the oft reported uncertainties in climate prediction resulting from cloud feedback (Dufresne and Bony 2008), ISCCP has emerged as a standard against which climate models are assessed (Zhang et al. 2005; Williams and Tselioudis 2007; Williams and Webb 2009).

Because the inputs to ISCCP algorithms (Rossow and Schiffer 1999) are visible channel reflectances and thermal infrared radiance measurements from weather satellites along with ancillary thermodynamic profiles, only a limited amount of unique information is available in any scene. Essentially, the visible reflectance is used to derive τ and the thermal infrared radiance is used to derive P_{top} when combined with a thermodynamic profile. These quantities then form the foundation for further analysis. Often joint histograms of P_{top} and τ are produced that are taken to describe the statistical characteristics of clouds in a region. It has been understood from the initial releases of ISCCP products that ambiguities associated with the retrieval of

Corresponding author address: Professor Gerald G. Mace, 201 S. 1460 E. Rm. 819 (WBB), Department of Atmospheric Science, University of Utah, Salt Lake City, UT 84112-0110.
E-mail: jay.mace@utah.edu

DOI: 10.1175/JCLI-D-12-00207.1

P_{top} and τ preclude their use in uniquely classifying an atmospheric column as containing one cloud type or another (Schiffer and Rossow 1983). These ambiguities are primarily because of the presence of multiple cloud layers of unknown infrared opacity and location in a vertical column. For instance, an optically thin cirrus layer over low stratus would have an infrared radiance that implies cloud tops somewhere between the geometric tops of either layer while the visible reflectance of the stratus would result in the assertion that the effective midtropospheric layer is optically thick. To overcome this ambiguity, it has been common practice to use a coarse histogram of nine P_{top}–τ bins to describe statistical distributions derived from ISCCP retrievals. For ease of understanding, these bins have been assigned names (Rossow and Schiffer 1999) that conform broadly to the nomenclature defined in 1802 by Howard (1804).

The use of ISCCP climatologies has taken on two general forms. The first is a straightforward comparison of model output statistics to similar ISCCP statistics after the model output has been passed through an algorithm simulating the ISCCP retrieval procedure (Klein and Jakob 1999; Webb et al. 2001). In essence, the simulator accounts for the fact that P_{top} is a radiative quantity that generally does not conform to a geometric definition of the pressure at the physical top of a cloud layer (Klein and Jakob 1999; Mace et al. 2011). Zhang et al. (2005) present a very thorough and oft cited example of this type of analysis. More sophisticated classes of analyses have emerged recently where all 42 bins of the ISCCP P_{top}–τ histograms are passed through clustering algorithms to identify cloud regimes. Jakob and Tselioudis (2003) pioneered this methodology and extended it to examine the vertical distributions of cloud occurrence at two geographic locations in the tropics where long-term cloud data had been collected [Jakob et al. 2005; see also Chen and Del Genio (2009)]. Since then, several important papers have emerged using variations of this technique to critically evaluate the global distribution of GCM-predicted ISCCP regimes against similar statistics compiled from ISCCP retrievals (Williams and Tselioudis 2007; Williams and Webb 2009). What has not been possible to know until recently is what the actual distributions of hydrometeor layers are within the various classifications defined by ISCCP P_{top}–τ statistics.

Active remote sensing with both terrestrial and spaceborne millimeter wavelength cloud radars and optical lidars can provide information regarding the actual vertical distributions of hydrometeor layers and their properties within ISCCP P_{top}–τ bins. For example, Jakob et al. (2005) use data collected at the Atmospheric Radiation Measurement (ARM) ground sites (Ackerman and Stokes 2003) to show that the ISCCP-defined regimes computed using statistical clustering algorithms over those sites have measureable interregime differences in cloud occurrence patterns. Jakob and Schumacher (2008) show these regimes also have measureable interregime differences in precipitation patterns. Chen and Del Genio (2009) extend the analysis at Manus and Nauru Islands by creating statistical regimes from the long-term cloud radar data in addition to regimes defined by ISCCP. They find that while the ISCCP regimes describe different meteorological conditions, there is ambiguity in the actual distributions of cloud occurrence and cloud properties within those regimes. In other words, a regime defined by cloud occurrences measured by cloud radar does not correspond uniquely to an ISCCP regime and vice versa [Fig. 8 of Chen and Del Genio (2009)]. This ambiguity also seems to extend to specific ISCCP regimes compared at different locations. For instance, the distributions of cloud occurrence in ISCCP regimes at Manus Island (2.1°S, 147.4°E) are different than the cloud occurrence patterns for the same regimes at Nauru Island (0.5°S, 166.9°E). The different geometric distributions of clouds for the same ISCCP regimes imply that the vertical structure of the cloud radiative properties at the two locations are such that the two distributions create similar P_{top}–τ statistics when viewed from space with thermal and visible channels. That regimes with different geometric cloud distributions appear radiatively similar simply underscores the nonuniqueness of results from a severely under constrained retrieval algorithm like ISCCP, given the natural variability of hydrometeors in the atmosphere.

While much detailed information can be derived from the suite of instruments at the ARM sites, the active remote sensing datasets produced by *CloudSat* and *Cloud–Aerosol Lidar and Infrared Pathfinder Satellite Observations* (*CALIPSO*) (CC) provide global hydrometeor layer occurrence information. Using large regional comparisons, Zhang et al. (2007) found that cluster analysis of *CloudSat* data produced regimes that had similarities to regimes produced by ISCCP data. Sassen and Wang (2008), who developed a cloud type classification algorithm using *CloudSat* data, present a comparison of cloud type with ISCCP types and show reasonable agreement on zonal averages for cloud types such as altostratus and stratocumulus but significant differences in others. Rossow and Zhang (2010) compared the vertical distribution of clouds from CC with a description of cloud vertical structure created by mapping a statistical representation of cloud layers derived from a radiosonde climatology (Wang et al. 2000) to ISCCP P_{top}–τ histograms (Rossow et al. 2005). This value-added ISCCP product was found in their comparison to CC to provide a meaningful climatological description of cloud vertical

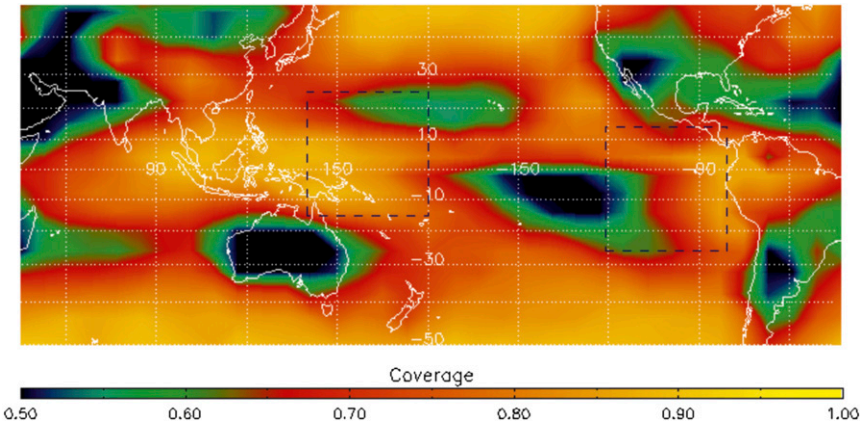

FIG. 1. Map showing the western and eastern Pacific study regions in the dashed outlined boxes. The background map shows the total cloud coverage derived from RL-GEOPROF for the 2007 and 2008 periods under consideration.

structure on regional scales. However, in a pixel to pixel comparison, Rossow and Zhang (2010) show that agreement between an ISCCP-derived description of cloud structure with what is actually observed by CC can only be expected about half the time, where agreement is defined by the two measurements being placed in the same P_{top}–τ histogram bin of the nine that have become common.

In this study, we build on the work of Rossow and Zhang (2010) and Chen and Del Genio (2009) to examine the vertical distributions of hydrometeor layers in two disparate regions of the equatorial Pacific.

2. Data and methods

We adopt a straightforward analysis approach. Using several *CloudSat* standard data products from calendar years 2007 and 2008, we examine regions that encompass 40° × 40° domains about the equator in the eastern and western Pacific (Fig. 1). We choose to consider two disparate climatically important regions in this initial study to fully illustrate the utility of using active remote sensing data to understand ISCCP statistics.

All data used in this study are from standard products produced by the *CloudSat* project and are available publicly at the *CloudSat* Data Processing Center (http://www.cloudsat.cira.colostate.edu). The hydrometeor layer occurrences from combined *CloudSat* radar and *CALIPSO* lidar data are available in the Radar–Lidar Geometrical Profile Product (RL-GEOPROF; Mace et al. 2009). The RL-GEOPROF dataset describes the vertical distribution of hydrometeor layers in footprints that are approximately 2.5 km in spatial scale along the *CloudSat* track. Atmospheric thermodynamic profiles are extracted from the European Centre for Medium-Range Weather Forecasts (ECMWF) data mapped to the *CloudSat* track in the auxiliary product known as ECMWF-AUX. We also use reflectance data from the Moderate Resolution Imaging Spectroradiometer (MODIS) that have been collocated to the *CloudSat* track in the MODIS auxiliary product (MODIS-AUX) and visible optical depths (τ) derived from MODIS reflectances in the *CloudSat* level-2B cloud optical depth product (2B-TAU) or from the MODIS atmosphere MYD06 product (Platnick et al. 2003).

The *CloudSat* Cloud Profiling Radar (CPR) and the *CALIPSO* lidar, when combined synergistically, are capable of identifying the vertical locations of most hydrometeor layers in the atmosphere (Mace et al. 2009). The CPR also has the distinct ability to map the vertical location of hydrometeor layers even in the presence of optically thick and lightly precipitating higher layers. Partial or full attenuation of the radar signal is possible in profiles that contain more than moderate ($>2\,\mathrm{mm\,h^{-1}}$) liquid precipitation. The lidar aboard *CALIPSO* is sensitive to optically tenuous hydrometeor layers and becomes fully attenuated in the presence of cloud layers with $\tau > \sim 3$. A significant synergy, however, is realized by combining the two active remote sensors. In addition to regions where the CPR is fully attenuated in heavy rain, another source of systematic bias in hydrometeor layer detection occurs when thin and usually liquid-phase layers that have reflectivity below the detection threshold of the CPR exist below optically thick layers that attenuate the lidar. Also because the CPR has minimal sensitivity below 1 km AGL as a result of the interaction of the radar pulse with the surface (Marchand et al. 2008), the CPR does not reliably detect layers that have tops below 1 km. Normally, the lidar is able to detect these layers except when the lidar is fully attenuated by higher clouds.

TABLE 1. Definition of the nine P_{top}–τ ISCCP diagnostic types.

	$\tau < 3.6\%$	$3.6\% < \tau < 23\%$	$\tau > 23\%$
High, $P_{top} < 440$ hPa	Cirrus	Cirrostratus	Deep Convection
Middle, $440 < P_{top} < 680$ hPa	Altocumulus	Altostratus	Nimbostratus
Low, $P_{top} > 680$ hPa	Cumulus	Stratocumulus	Stratus

These detection biases are not thought to significantly influence the general findings of this study.

To simulate what ISCCP would diagnose in each vertical profile, we average seven *CloudSat* footprints to approximately simulate the spatial scales of ISSCP satellite measurements. To each averaged profile we implement a component of the ISCCP simulator algorithm (Klein and Jakob 1999; Webb et al. 2001) known as ISCCP Clouds and Radiances Using SCOPS (ICARUS), where SCOPS is the Subgrid Cloud Overlap Profile Sampler—the ISCCP simulator component that we do not use for this study. SCOPS statistically subsamples the vertical cloud fraction and cloud properties predicted by a model at the model grid-scale resolution using the model's cloud overlap assumption. The ISCCP P_{top} is calculated at the averaged *CloudSat* footprint scale. Because ISCCP is generally insensitive to optically thin cirrus layers that are ubiquitous in the western Pacific in the tropical tropopause transition layer (Schwartz and Mace 2010), all cirrus with bases above 15 km with total optical depth of less than one are excluded from the analysis.

ICARUS consists of several components designed to use atmospheric simulations of cloud and thermodynamic properties in order to calculate P_{top}. The three components used from the original simulator for this study include a tropopause locator, a column effective temperature simulator, and a cloud-top pressure simulator. The tropopause locator uses the temperature profile from ECMWF-AUX to locate the pressure level and temperature of the tropopause, a necessary step for the calculation of column IR emissivity. The tropopause temperature, the clear and cloudy 10.5-micron radiances, and the column optical depth are used as input to the ISCCP brightness temperature simulator. The *CloudSat* MODIS-AUX product provides observed cloudy radiances and the clear-sky radiances are calculated using the infrared radiative transfer model described by Christi and Gabriel (2004) known as Radiant using the ECMWF-AUX thermodynamics following the implementation of that model described by Cooper et al. (2006). Column optical depths when not available from MODIS products are derived using techniques described in Mace (2010). The effective radiative temperature of a footprint is then referenced to a pressure level to arrive at the pressure that ISCCP would purportedly diagnose P_{top}. Using long-term statistics from an ARM site, Mace et al. (2011) evaluated the validity of the ICARUS algorithms and found that ICARUS provides a reasonable simulation of the P_{top} reported by the ISCCP product. Each *CloudSat* profile then is assigned a simulated P_{top} and τ as ISCCP would retrieve, as well as the actual geometric cloud top(s) and base(s) reported by the merged *CloudSat–CALIPSO* mask in RL-GEOPROF. The P_{top} and τ information is then organized in joint histograms following Rossow and Schiffer (1999), and the vertical distributions of the observed hydrometeor layers within these P_{top} and τ bins are examined.

We adopt the following terminology to discuss various aspects of the cloud climatologies: we typically use classifications defined by ranges of P_{top} and τ that have become standard [Table 1 and Rossow and Schiffer (1999)]. When referring to one of these nine types, we capitalize the term used to define it. For instance, for $P_{top} < 440$ hPa and $\tau < 3.6$, we refer to the ISCCP Cirrus type (note the capitalization); and for $P_{top} > 680$ hPa and $\tau < 23$, we refer to the ISCCP Stratus type. When we discuss a certain range of P_{top} without regard for τ, we refer to ISCCP High, Middle, and Low types. Each of these ISCCP types have a frequency of occurrence (RFO) relative to the number of cloudy columns sampled by CC in the analysis regions during the 2-yr period under consideration. The fraction of cloudy columns is referred to as the CF and includes columns with hydrometeors anywhere in the vertical (excluding layers based above 15 km with optical depth less than 1). Later, we show joint histograms of frequencies of occurrence of certain geometrically defined layers. The frequency of a certain class of hydrometeor layer within the joint histograms is discussed in terms of its relative frequency of occurrence within that histogram (RRFO) where the frequencies of all layers within a histogram sum to 1. We at times also refer to the absolute frequency of occurrence (AFO), defined as the number of times a certain phenomenon occurs normalized by the total number of columns, cloudy and cloud free, observed by CC in an analysis region during the analysis period (2007/08).

As an example, Fig. 2a shows data collected on 10 January 2007 over the west Pacific study region. A diversity of cloud types can be identified in this cross section, including isolated convection near 7°S and just north of the equator as well as deeper convection with thick anvils beginning at 5°S. Also evident are thicker

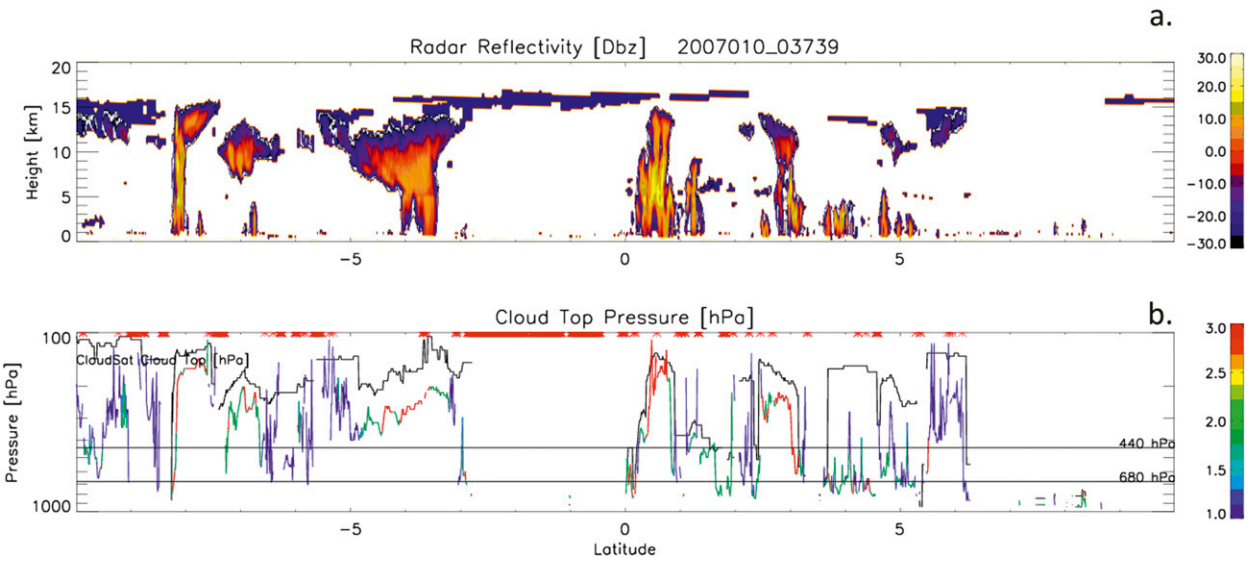

FIG. 2. Example ICARUS results along a curtain of A-Train data in the west Pacific study region. (a) Combined *CloudSat* radar reflectivity and *CALIPSO* lidar occurrence data from the RL-GEOPROF product. The volumes that are below the sensitivity of *CloudSat* are shown as reflectivity values of -32 dBZ_e (color bar on right). (b) Results of applying the ICARUS component of the ISCCP simulator to the data in (a). The black curve indicates the observed data from RL-GEOPROF, and the colors indicate the optical depth of the columns considered with blue indicating $\tau < 3.6$, green $3.6 < \tau < 23$, and red $\tau > 23$. The red symbols across the top of (b) indicate where ICARUS found no solution. Cirrus based above 15 km with $\tau < 1$ are neglected. Negative latitudes are south of the equator.

areas of cirrus as well as isolated shallow boundary layer clouds, some of which are several kilometers deep and would likely be classified visually as cumulus congestus. In several locations, cirrus exists over the boundary layer clouds. The results of the ICARUS algorithm are shown with the actual CC cloud tops in Fig. 2b. We find that for the optically thick layers that are topped with tenuous ice layers, the effective radiative cloud top is generally several hundred hectopascals lower than the actual top, although in most cases the cloud layer would still be classified as a high cloud (i.e., $P_{\text{top}} < 440$ hPa) in the 9-bin histogram method. Only in the very thick convection just north of the equator, where the W-band 10-dBZ reflectivity extends to near the geometric layer top, does the simulated ISCCP value come within a few tens of hectopascals of the geometric top. Alternatively, where cirrus overlay boundary layer clouds, the solution found by ICARUS depends on the radiative properties of the cirrus layer. When the cirrus are optically thick, the simulated P_{top} is often in the upper troposphere, while for thin cirrus P_{top} is assigned an intermediate pressure value. For thin cirrus existing alone in the column, the simulator often finds a solution that would classify the column as cumulus with $P_{\text{top}} > 680$ hPa.

The ICARUS P_{top} (i.e., the radiative cloud top) causes a much broader variation in the joint 42-bin P_{top}–τ histogram when compared with the RL-GEOPROF layer top boundaries, as shown in Fig. 3. Note that both figures share the same visible optical depth so that the only difference between the two is the way P_{top} is defined. The active remote sensors find the majority of the cloud layers to have P_{top} less than 300 hPa. While the ISCCP-simulated distribution of P_{top} (again, the radiative cloud top) is predominantly less than 440 hPa, the distribution is weighted to higher values of P_{top}. Also, many of the columns with actual high clouds are diagnosed to have middle and lower-tropospheric cloud-top pressures.

3. Hydrometeor layer statistics in the study regions

Historically, clouds have been defined in terms of their base heights and layer thicknesses as well as their general character (cumuliform, stratiform, etc.; World Meteorological Organization 1975). The broad use of this nomenclature has carried through to the satellite era and it influences the manner in which ISCCP statistics and even A-Train data are interpreted (i.e., Williams and Webb 2009; Sassen and Wang 2008). We therefore begin with a description of the geometric hydrometeor occurrence statistics in the two study regions (Figs. 1, 4, and 5) from the active remote sensors on the A-Train.

The analysis regions as shown in Fig. 1 are overlain on the 2007/08 hydrometeor layer coverage map derived from CC measurements. The domains were chosen to encompass widely varying cloud genre that naturally occur in each region. We attempted to avoid, to the extent

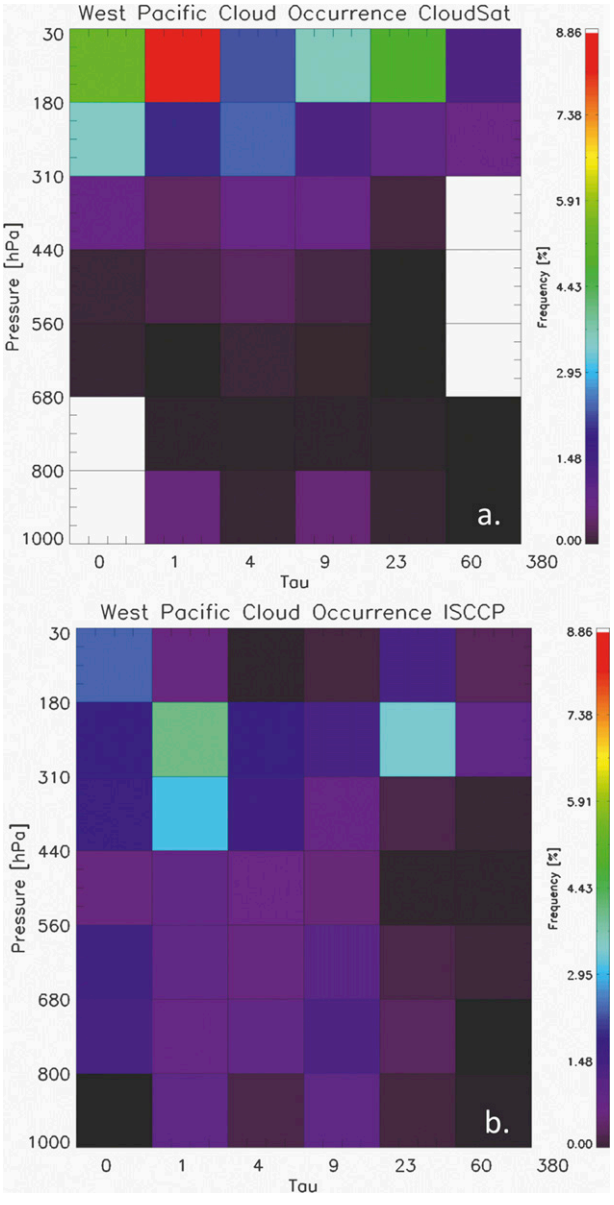

FIG. 3. The P_{top}–τ joint histograms from Fig. 2. (a) Observed from RL-GEOPROF and retrieved 2B-TAU *CloudSat* products. (b) Resulting P_{top}–τ joint histogram after application of the ICARUS algorithm to the observations.

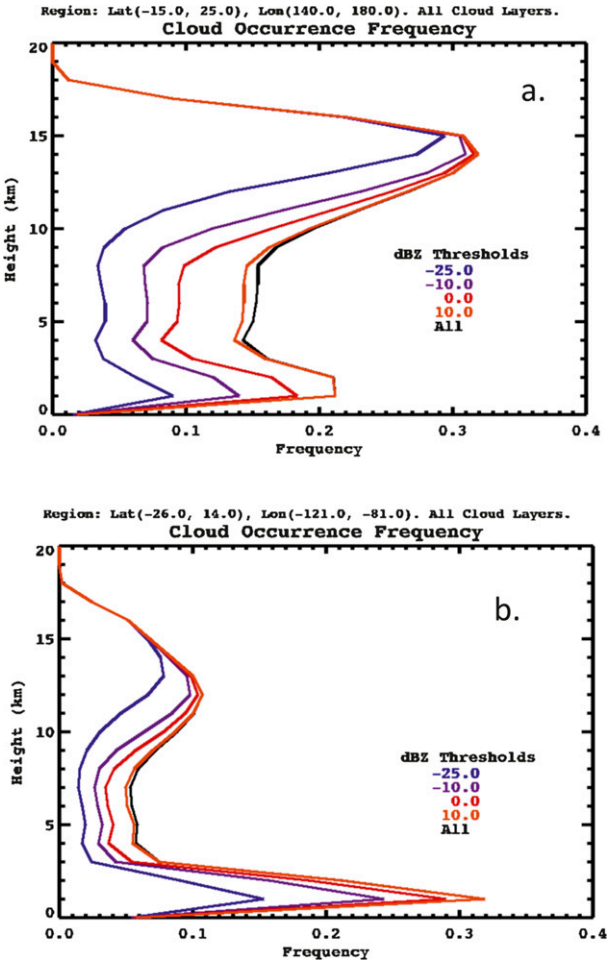

FIG. 4. Hydrometeor occurrence frequency from the RL-GEOPROF product as a function of height in (a) the west Pacific study region and (b) the east Pacific study region for the years 2007 and 2008. The colored curves show the occurrence frequency for all observations with radar reflectivity less than the value indicated in the legend.

possible, large landmasses that had a strong diurnal cycle. Regions of deep convection are included over the western Pacific warm pool and in the Panama Bight and the eastern Pacific ITCZ. Regions of shallow marine clouds are also included as the analysis domains extend northward and southward in the west and east, respectively, into areas dominated by shallow marine clouds and sparse cloud coverage. Figures 4 and 5 show, however, that the large-scale dynamics of the Walker circulation result in disparate vertical occurrence frequency profiles. The west Pacific study region exists in the upwelling portion of the Walker circulation, where warm sea surface temperatures contribute to the production of widespread deep precipitating clouds and an extensive coverage of cirrus. By contrast, in the east Pacific, a cooler sea surface and large-scale subsidence results in shallower convective clouds, less precipitation, and less cirrus. The east Pacific ITCZ does migrate through this domain, and summer season convection is strong and widespread in the Panama Bight region. The vertical distributions of radar reflectivity and layer statistics clearly reveal the broad hydrometeor characteristics of these regions that result from their contrasting large-scale dynamics. In the west Pacific, where the total cloud cover is found to be 77% (41% of the 6.5 million cloudy columns collected by *CloudSat* from 2007 through 2008 were multilayered), not only do we find

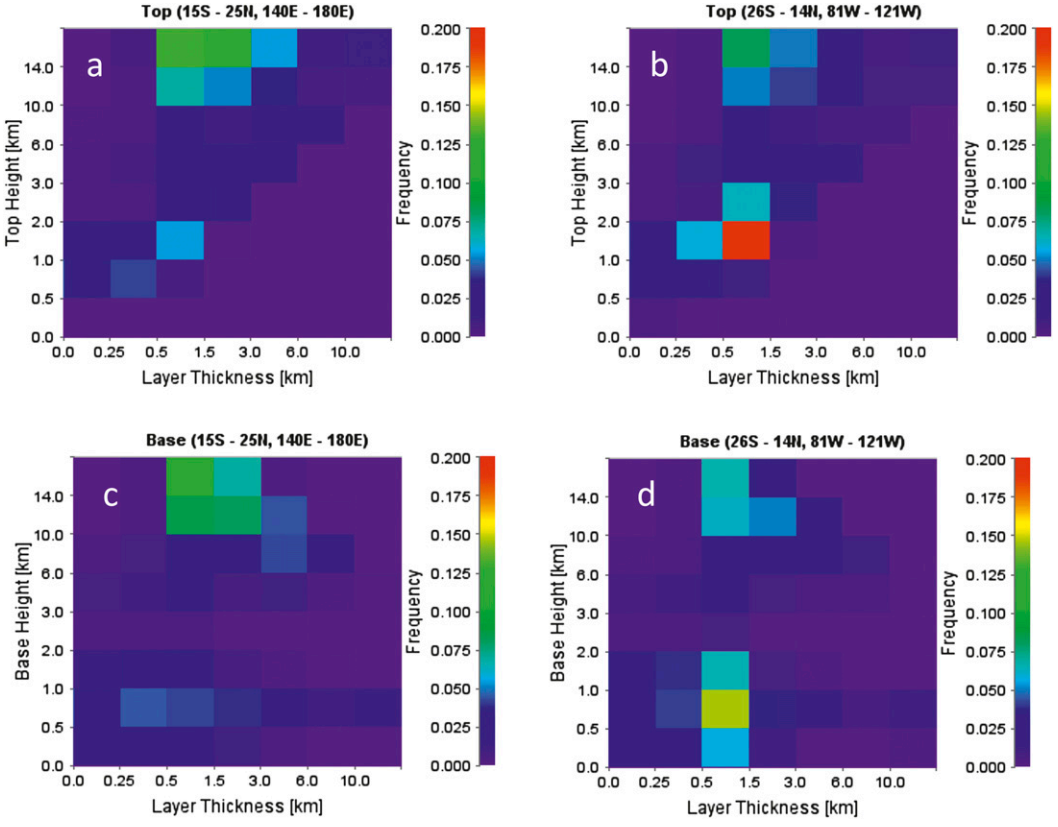

FIG. 5. (a),(b) Hydrometeor layer top height and (c),(d) hydrometeor layer base height by layer thickness histograms for the (left) west Pacific study regions and (right) east Pacific study regions compiled from the 2007/08 RL-GEOPROF data.

a larger occurrence of hydrometeors in the midtroposphere, but also a greater fraction of these clouds occur at larger values of radar reflectivity indicative of more extensive precipitation. Note that as much as half of the hydrometeor occurrences in the midtroposphere are found to have W-band radar reflectivity factors in excess of $+10\,\mathrm{dB}Z_e$. In the east Pacific where the total cloud cover is 71% (25% of the 5.9 million cloudy columns were multilayered), the vertical distribution of hydrometeor occurrence is distinctly bimodal, and there is much less indication of precipitation in deep clouds in the midtroposphere.

The joint base height–layer thickness and top height–layer frequency histograms (Fig. 5) provide a more detailed picture of the cloud climatologies of these regions. For the geometrically thin layers (less than 3 km) that compose the vast majority of the hydrometeor layers in both the east and west Pacific study regions, what we learn from the base and top histograms are similar. The fractional occurrence of clouds based in the boundary layer is about a factor of 2 larger in the east Pacific study region (51% of all profiles) than in the west Pacific study region (27%). The numbers are nearly reversed for high clouds (based above 6 km) with approximately 45% coverage in the west and 25% coverage in the east. For thicker layers, the base height histograms are interpreted more easily than the top height histograms. Moderately thick layers (1.5–6 km in thickness) based below 2 km likely represent cumulus congestus and are nearly identical in occurrence frequency between the west and east. Deep clouds, on the other hand, that include raining stratiform regions and deep convection (bases below 1 km and thicknesses greater than 6 km) compose roughly 5% of the profiles in the west and 3% in the east. Deep cirrus (bases above 6 km and thickness greater than 3 km) are much more frequent in the west with a 10% frequency compared to 5% in the eastern Pacific.

The predominance of high clouds in the west Pacific and low-level layers in the east Pacific carries through to the 42-bin P_{top}–τ joint histograms (Fig. 6), where we use only the uppermost layer top to define the observed P_{top} (Figs. 6b,d). Recall also that we have excluded layers based above 15 km with $\tau < 1$. Layers with the smallest values of P_{top} (<310 hPa) are the most frequent P_{top}–τ type in the western domain joint histogram. The high-topped cloud distribution seems to be bimodal with notable

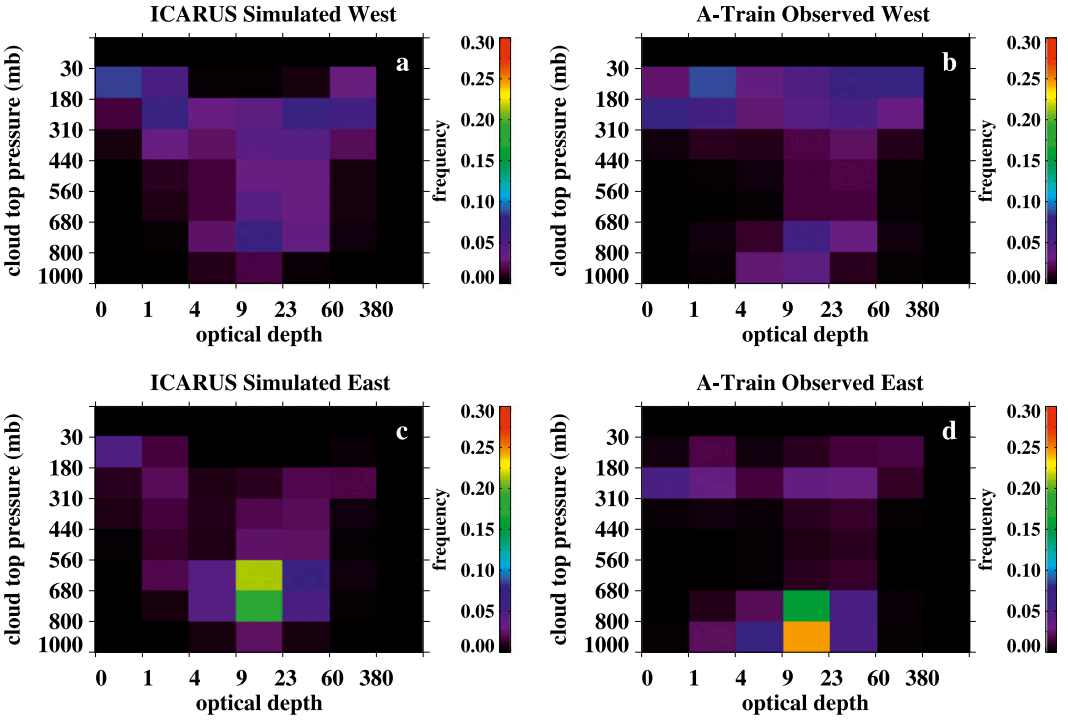

FIG. 6. The P_{top}-τ joint histograms from data collected during years 2007/08 from the (a),(b) west Pacific study regions and the (c),(d) east Pacific study regions. Panels (a) and (c) show the results of applying the ICARUS component of the ISCCP simulator to the A-Train measurements and (b) and (d) show observations from RL-GEOPROF.

maxima for $\tau < 4$ and $\tau > 23$. In the east, where there is much less coverage of cirrus and a higher coverage of boundary layer clouds, the P_{top}–τ joint histogram is more descriptive of the geometrically defined cloud climatology. The distribution of P_{top}–τ in the east Pacific depicts two maxima, one for upper-tropospheric clouds and one for the predominate boundary layer cloud type that has $P_{top} > 800$ hPa and $4 < \tau < 60$.

Applying ICARUS to the RL-GEOPROF data tends to redistribute cloudy columns throughout the joint histogram space. These results are in broad qualitative agreement with ISCCP statistics compiled for similar study domains by Hartmann et al. (2001; their Figs. 2 and 7). The ICARUS-simulated joint histogram for the west Pacific (Fig. 6a) has maxima in occurrence distributed throughout all P_{top} bins. The maximum at the top left-hand corner of Fig. 6a is an artifact of the ISCCP cloud identification: like the ISCCP retrieval algorithm, if ICARUS is not able to classify a column based on the input data, it is assumed to be thin cirrus and placed in the P_{top}–τ bin with the lowest pressure and lowest optical depth. In both domains, ICARUS causes much of the cirrus to be placed in larger P_{top} bins (lower in geometric height). This occurs even for layers that would be considered optically thick. Even though these layers are indeed opaque to visible and IR radiation when considered as an entity, they are often vertically extended and the tops of the layers are quite tenuous. The tenuous nature of the upper regions of these layers results in significant biases in cloud-top height estimates from passive measurements (Weisz et al. 2007).

In the east Pacific, however, the predominant boundary layer clouds are moved geometrically upward in height mostly to the next smallest set of P_{top} bins. This occurs because the ICARUS algorithm, as well as ISCCP, identifies the first occurrence moving downward from the tropopause in the thermodynamic profile of the effective cloud-top temperature as P_{top}. The first occurrence of the effective temperature is often the top of the persistent marine inversion, even though most of the boundary layer clouds reach their maximum physical height near or below the base of the inversion. This artifact is assumed to not result in significant errors because the set of bins nearest the surface includes $P_{top} < 680$ hPa. There is, however, a nontrivial fraction of these marine clouds that are placed into the midlevel bins.

4. Hydrometeor layers within P_{top}–τ joint histograms

We separate the ISCCP-simulated data into simplified regimes by reducing the 42-bin joint histograms into the

coarser 9-bin version following Rossow and Schiffer (1999) and others. The terminology that has become common for this 9-bin representation of ISCCP data is defined in Table 1. There are a number of ways of representing the A-Train geometric layer distributions within the ISCCP P_{top}–τ histogram space. We display the joint relative frequencies of occurrence of layer bases and layer thicknesses that were observed by CC in vertical columns that were diagnosed by ICARUS to have P_{top}–τ top-of-atmosphere (TOA) radiative signatures specific to the types listed in Table 1. The joint histograms for the western and eastern Pacific study regions are shown in Figs. 7 and 8, respectively. A scan of the joint distributions of layer base and layer thickness shows that while certain P_{top}–τ types faithfully represent a specific genre of hydrometeors, many of the ISCCP P_{top}–τ types are composed of some combination of a predominant cloud type and other layers. In these situations, hydrometeor layer populations that extend in varying degrees throughout vertical columns statistically characterize the TOA radiative signatures that define an ISCCP type, and a narrow interpretation of an ISCCP type as a single genre of clouds must be carefully assessed. More specifically, we find that clouds based in the boundary layer are a prominent feature of all the ISCCP types with the exception of Cirrus. What seems to vary from type to type is the occurrence frequency of high layers and the geometrical thicknesses of the layers overall.

Moving across the top rows of Figs. 7 and 8, the ISCCP high clouds show a monotonic progression from geometrically thin upper-tropospheric layers to geometrically thicker layers based at lower altitudes. The Cirrostratus type is often (~40%) associated with layers that are based at pressures exceeding 440 hPa. Especially for the geometrically thinner layers in the upper troposphere, the classification of ISCCP Cirrostratus is often associated with the presence of a highly reflective lower cloud layer underlying the geometrically thin cirrus. We find that for the Cirrostratus type highly reflective layers with tops exceeding 440 hPa are found approximately 25% of the time in both analysis regions. In the Deep Convection type in both regions, geometrically thick layers (>10 km) based in the lower troposphere are notable and have RRFOs of approximately 75%. These deep layer frequencies equate to AFOs of approximately 1% in the east and 3% in the west, and they are composed of deep convection and raining stratiform layers. In both study regions, we find that layers based at pressures lower than 680 hPa compose approximately 25% of the layers in the Deep Convection type.

The ISCCP midtropospheric types that have RFOs of 38% in the east and 20% in the west are composed of very little actual midtropospheric cloud layers. Hydrometeor layers with tops in the upper troposphere are found between 20% and 50% of the time in all but the Altostratus type in the east. The occurrence of higher topped layers is more frequent in the western study region. Considered broadly, it appears that the principal differences between the vertical distributions of hydrometeor layers in the mid- and lower troposphere ISCCP types are the relative fractions of layers based in the upper troposphere. In both regions, the midtroposphere ISCCP types tend to have a higher population of layers in the upper troposphere. In the east, many of the lower-tropospheric layers that are ultimately classified as being midtropospheric clouds occur because the layers are erroneously placed at the top of the trade inversion. Regardless of the reasons, the results in Figs. 7 and 8 suggest that the midtroposphere ISCCP types are typically not associated with layers that actually occupy the region between 680 and 440 hPa. The Stratus and Stratocumulus types contain less cirrus and more low-level clouds than are found in the middle types. This is particularly true in the east where there is less cirrus overall.

5. Discussion

The ISCCP diagnostic products have been used extensively to explore the effects of clouds on Earth's energy balance and for evaluation of global climate models. Many of these studies parse the ISCCP statistics into the nine P_{top}–τ types and then examine the relative spatial distributions of these types in comparison to those produced by models (e.g., Weare 2004; Zhang et al. 2005) and/or attempt to evaluate the influence of certain cloud types on the surface and atmospheric energy budgets (e.g., Hartmann et al. 2001; Raschke et al. 2005; Chen et al. 2000). While we know that TOA radiative effects of a certain ISCCP type are similar by definition, TOA similarity does not necessarily imply similarity in other characteristics such as vertical distributions of layers, radiative heating profiles, or surface radiative forcing (Stephens and Webster 1984). In other words, such interregional evaluations of ISCCP statistics implicitly assume that similarity in TOA radiative signatures imply similarity in terms of cloud morphology defined in other ways. For example, the assumption is often implicit that the atmospheric columns classified in the ISCCP Altostratus type in one region are similar to columns classified as Altostratus in other regions. Similarity among statistical distributions can be quantified and assumptions of similarity can be tested quantitatively. The active remote sensors of the A-Train provide a unique opportunity to quantitatively evaluate these assumptions of similarity for the ISCCP types.

To test the statistical similarity of the P_{top}–τ-defined ISCCP types in the western and eastern Pacific study

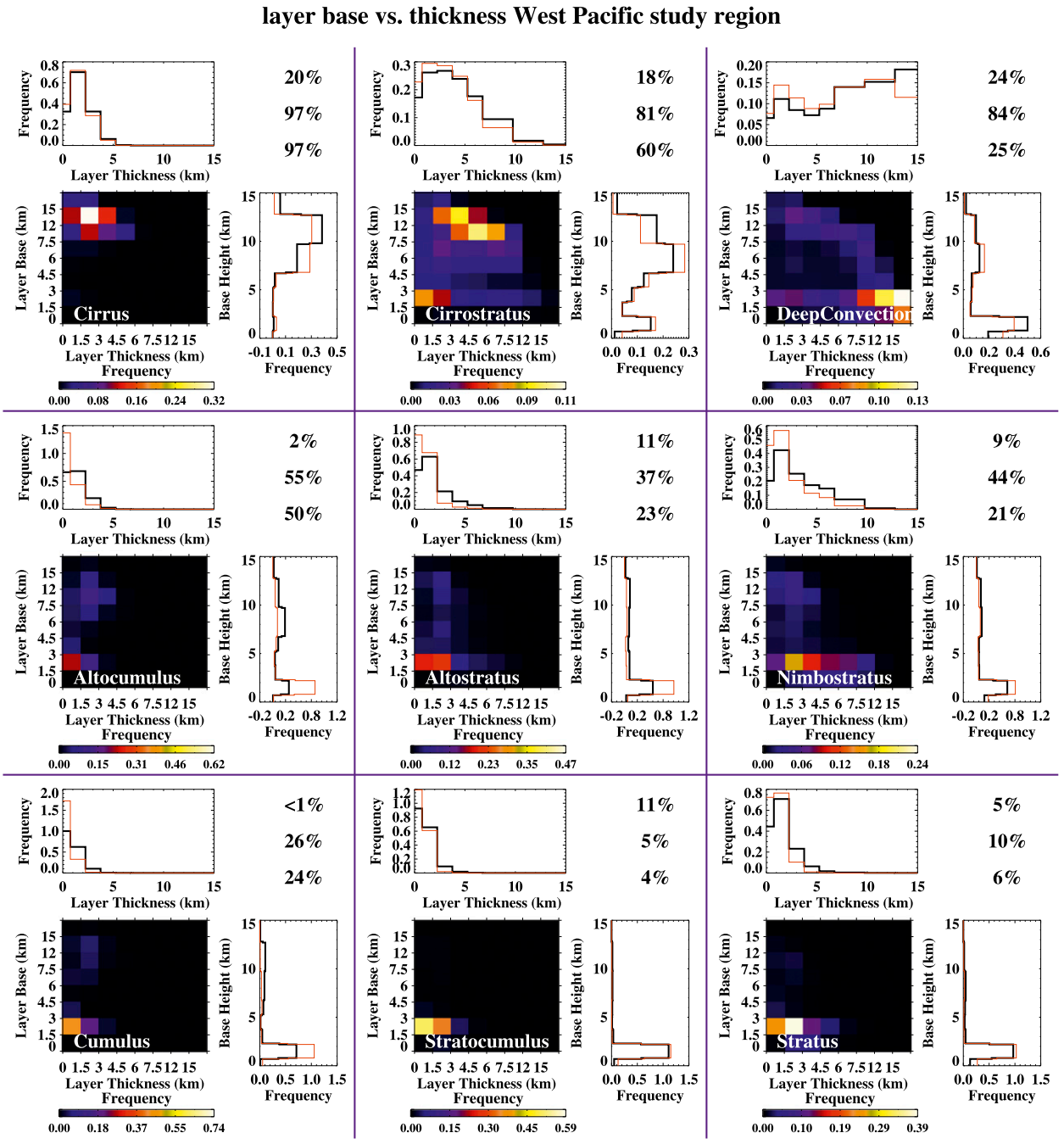

FIG. 7. Distributions of hydrometeor layers within the ISCCP P_{top}–τ 9-bin representation in the west Pacific study region during 2007/08. For each ISCCP type (defined in Table 1) a conditional distribution of layer base and layer thickness is shown, as in Figs. 5a and 5b. To the right of each conditional distribution is the frequency of cloud base as a function of height and above each conditional distribution is the frequency distribution of layer thickness. The solid black histograms represent the western study region and the thin orange lines show the eastern study region for comparison. The three numbers in the top right of each cell show the relative frequencies of occurrence of each ISCCP type as produced by ICARUS, the middle percentage gives the fraction of layers observed by CC that have layer tops above 440 hPa when that column is diagnosed by the ISCCP simulator to be found in that P_{top}–τ category, and the bottom number shows the fraction of layers where layers bases are found above 440 hPa.

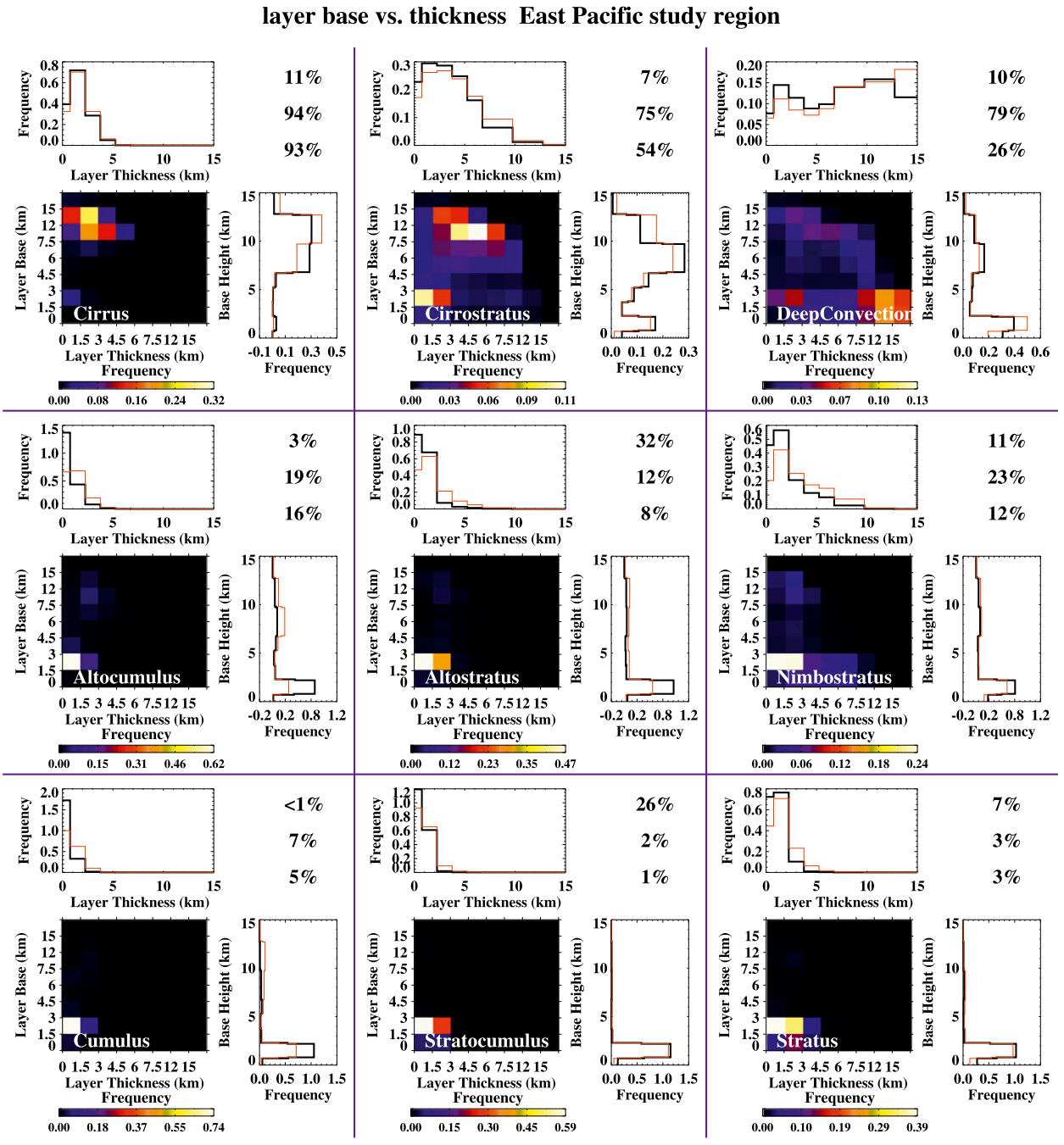

FIG. 8. As in Fig. 7, but for the east Pacific study region during years 2007/08.

regions, we subject the layer base and top joint distributions of specific P_{top}–τ regimes to Kolmogorov–Smirnov (K–S) statistical tests as described in Peacock (1983) and further evaluated in Lopes et al. (2007). The K–S statistic uses differences in the cumulative probability distributions of two samples to quantify the likelihood that the two samples are drawn from similar populations. It can be shown that if two samples are drawn from the same population, then the maximum difference $D^{max}_{similar}$ in their cumulative distribution functions is expected to be $1/\sqrt{N_e}$, where N_e is the effective number of independent measurements. The test statistic $Z_{similar} = D^{max}_{similar}\sqrt{N_e}$, whose sampling distribution is well known for large N_e, allows for a determination of the probability p that $Z_{similar}$ is greater than a value of Z derived from two measured distributions. As p becomes larger it is more

TABLE 2. Results of the K–S statistical tests comparing the hydrometeor layer distributions in the eastern and western Pacific study regions for the nine P_{top}–τ ISCCP diagnostic types defined in Table 1. The term Z_x gives the K–S statistic produced by comparing the measured distributions where rows labeled 2D refer to the two-dimensional joint distributions of layer base and layer top observed by CC, and rows labeled base, top, and thick refer to the one-dimensional vertical distributions of layer base height, layer top height, and layer thickness. The term p gives the probability that the theoretical K–S statistic Z defined for distributions drawn from the same population is greater than the measured value of Z_x. When $p < 0.01$, we can reject the null hypothesis at greater than 99% confidence. In other words, we can confidently state that the two hydrometeor populations when geometrically defined by active remote sensors are statistically dissimilar from one another. Columns labeled $\widehat{N}$ give the results of the independent sample test described in the text, and columns labeled $\widehat{F}$ give the results of the replacement test described in the text. Boldface font indicates distributions for which the null hypothesis that the measured distributions are drawn from identical populations cannot be rejected at the 99% confidence level.

	Z_x	p	$\widehat{N}$	$\widehat{F}$	Z_x	p	$\widehat{N}$	$\widehat{F}$	Z_x	p	$\widehat{N}$	$\widehat{F}$
	East–west Cirrus				East–west Cirrostratus				East–west Deep Convection			
2D	2.5	10^{-4}	200	0.85	**1.2**	**0.22**	—	—	**0.89**	**0.64**	—	—
Base	**1.3**	**0.07**	—	—	**0.88**	**0.4**	—	—	**0.89**	**0.40**	—	—
Top	2.5	10^{-5}	200	0.65	**1.1**	**0.15**	—	—	**0.34**	**0.99**	—	—
Thick	**1.6**	**0.01**	—	—	**0.63**	**0.8**	—	—	**0.95**	**0.33**	—	—
	East–west Altocumulus				East–west Altostratus				East–west Nimbostratus			
2D	4.6	10^{-16}	60	0.3	4.9	10^{-18}	60	0.35	3.7	10^{-9}	150	0.50
Base	4.7	10^{-19}	40	0.3	4.7	10^{-19}	60	0.30	3.7	10^{-12}	100	0.45
Top	4.4	10^{-17}	60	0.3	3.9	10^{-13}	100	0.40	**1.6**	**0.01**	—	—
Thick	2.0	10^{-4}	200	0.8	2.9	10^{-7}	150	0.60	2.8	10^{-7}	150	0.6
	East–west Cumulus				East–west Stratocumulus				East–west Stratus			
2d	3.7	10^{-11}	100	0.45	**1.5**	**0.07**	—	—	2.7	10^{-5}	200	0.75
Base	3.7	10^{-9}	90	0.4	**1.4**	**0.03**	—	—	2.5	10^{-6}	200	0.65
Top	2.7	10^{-9}	200	0.5	**0.93**	**0.35**	—	—	**1.3**	**0.08**	—	—
Thick	**1.6**	**0.01**	—	—	**0.82**	**0.50**	—	—	1.8	10^{-3}	300	0.90

likely that the two measured distributions are drawn from the same population (the null hypothesis). As commonly implemented (Press et al. 1992), we reject the null hypothesis when $p < 0.01$ (i.e., 99% confidence) and state that the two distributions are likely *not* drawn from the same population. To utilize the full information provided by the active remote sensors of the A-Train, we implement both the one- and two-dimensional versions of the K–S test described by Peacock (1983) and list Z_{mea} and p as Z_{2d} and p_{2d} in Table 2. We also quantify the K–S statistics of the one-dimensional (1D) frequency distributions of layer base, layer top, and layer thickness dz and list them in Table 2 as Z_x and p_x, where subscript x is the appropriate 1D distribution (top, base, and dz).

To develop reasonable evaluations of similarity for this purpose, two modifications to the CC measurements are made. First, the vertical resolution of the CC data must be coarsened to match the native resolution of ISCCP by converting the seven P_{top} boundaries and their bin centers to geometrical height using the hypsometric equation and then assigning all layer bases and tops measured by CC to the nearest ISCCP bin center height. The other issue, not so easily dealt with, is the number of independent samples that exist in the multiyear dataset. Because the active remote sensors provide along-track samples every 2.5 km and the spatial scales of cloud systems in these regions are highly variable, there are clearly much fewer independent samples than there are columns measured. Therefore, to be as conservative as possible we reduce the number of independent samples to 1 day^{-1} from the $>10^6$ profiles collected in each region. Both of these adjustments have the effect of improving the likelihood that we accept the null hypothesis that a given hydrometeor distribution in one location for a P_{top}–τ regime is statistically similar to the hydrometeor distribution from the same P_{top}–τ regime in another region.

While Z and p taken together provide information regarding the similarities of the statistical distributions of hydrometeor layer properties in the ISCCP P_{top}–τ regimes, beyond the statement of accepting or rejecting the null hypothesis, the interpretation of Z and p is not exceedingly intuitive. Therefore, we conduct two exercises using the K–S test that provide relative and perhaps more intuitive measures of the degree of similarity of the hydrometeor layer statistics for given ISCCP types. The first of these is straightforward and entails incrementally decreasing the number of independent samples N that are specified in each comparison from the assumed value of 730 discussed above. Because for two distributions Z_{mea} is inversely proportional to $\sqrt{N}$, p_x becomes smaller as N increases. The value of N where $p_x < 0.01$ (hereafter referred to as $\widehat{N}$) provides information on the relative (dis)similarity of two distributions. This test is illustrated in Fig. 9a by comparing

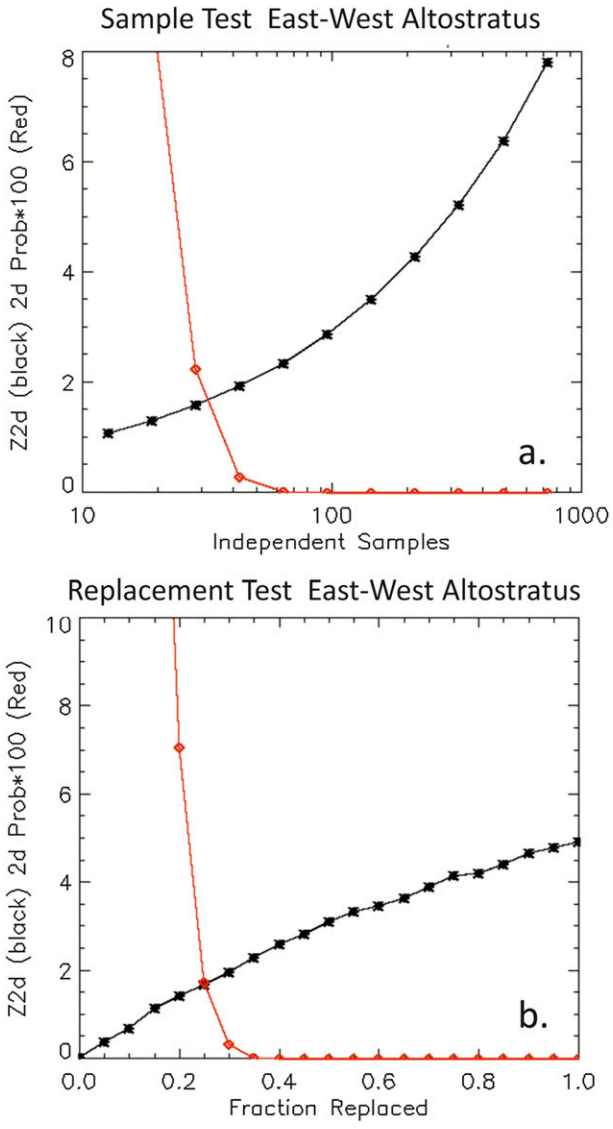

FIG. 9. Examples of (a) the independent sample test and (b) the replacement test discussed in the text. Shown are comparisons of the 2D joint histograms of layer base and top for the ISCCP Altostratus type in the eastern and western study regions. The red lines denote the value of p that indicates the probability (times 100) that the Kolmogorov–Smirnov statistic Z_{similar} derived from distributions drawn from identical populations is greater than a value of Z_{2d} (the black lines) derived from two measured distributions.

the joint layer base and top distributions that are observed by CC when ICARUS diagnoses the Altostratus type. Using 730 independent samples, we find that the null hypothesis can be confidently rejected and conclude that the geometrical distributions of hydrometeor layers when ISCCP diagnoses Altostratus are drawn from different populations of hydrometeors. In simpler words, ISCCP Altostratus in the west and east are not the same cloud population when defined geometrically. Reading Fig. 9a from right to left, as we incrementally reduce the number of independent samples by a factor of 1.5 at each step, we find that p_{2d} first rises above the significance level of 0.01 for $N = \hat{N} \simeq 60$. So, a factor of about 10 fewer independent samples must be assumed to conclude that the hydrometeor layers occupying the Altostratus types in the two regions are drawn from some common cloud population. While this number ($N = \hat{N} \simeq 60$) has no physical meaning, it does provide a relative measure of the degree of similarity between the two cloud populations defined to be Altostratus using ISCCP P_{top}–τ criteria.

The second exercise is somewhat more complicated to describe, but the results, we believe, provide more information. Consider two distributions of some hydrometeor layer property x from the eastern and western study regions where $p_x < 0.01$ and the null hypothesis that the distributions are drawn from the same population can be rejected. One of those distributions will have fewer members than the other. For the sake of description, assume that the eastern distribution has fewer members than the western distribution. If we construct a new distribution—in lieu of the eastern distribution—that has the same number of members as the eastern distribution but is randomly populated with measurements from the larger western distribution, we would find that the new distribution is statistically indistinguishable from the western distribution. Now, if we incrementally replace some fraction of members F of the new distribution with measurements randomly pulled from the eastern distribution, we can identify a value of F ($\widehat{F}$) where the null hypothesis can first be rejected (i.e., where the two distributions appear confidently to have been drawn from different hydrometeor populations). The more dissimilar the original distributions are from one another, the smaller $\widehat{F}$ will need to be before $p_x < 0.01$ and the null hypothesis is rejected. The value $\widehat{F}$ then, like $\widehat{N}$, provides a relative measure of the degree of (dis)similarity of the two distributions.

Figure 9b provides an illustration of the replacement test. Here, the new distribution is constructed to have the same number of members as the Altostratus joint distribution in the east, but it is fully populated with members from the west. When that new distribution is compared to the full joint distribution of layer bases and tops from the west, we find that the two distributions are statistically indistinguishable. As we incrementally replace the members of the new distribution with measurements from the eastern study region, we find that two distributions become increasingly dissimilar. The null hypothesis is finally rejected when $F = \hat{F} \simeq 0.3$. In other words, 30% of the new distribution contains measurements of layer bases and tops from the east when the null hypothesis is rejected.

The results of comparing the western region ISCCP types with the same eastern type are summarized in

Table 2. For the most part, these statistics validate the qualitative interpretation arrived at by examining the joint distributions in Figs. 7 and 8. Overall, we find that the degree of similarity of the ISCCP types between the two study regions is generally greatest for the high types and is lowest for the middle types. The null hypothesis cannot be rejected for the Cirrostratus and the Deep Convection types. In other words, the geometric distributions of layers within the two study regions appear to be drawn from a common population. The principle difference in the Cirrus type is the layer tops. The optically thin high clouds in the western study region tend to be found at lower P_{top} or greater geometrical heights than in the eastern study region. Otherwise, the layer base and thickness distributions appear statistically similar to one another.

Rejection of the null hypothesis is much more certain for midlevel types. In the replacement tests, $\widehat{F}$ is found to be in the 0.3–0.5 range, suggesting that the populations diverge when less than ⅓–½ of the layers are substituted. The independent sample tests provide similar results, with $\widehat{N}$ ranging from 60 to 100. Of the measures of similarity, the layer thickness distributions appear the least dissimilar, and the Nimbostratus types appear more statistically similar than do Altocumulus and Altostratus. The statement regarding layer thickness actually holds true for most of the nine types considered. Because the geometrical thickness is a strong determinant of the optical thickness, classification by optical thickness also classifies by geometrical thickness to some degree. Comparing the midtropospheric joint distributions in Figs. 7 and 8, we see that our rejection of the hypothesis that the types are drawn from a common population of layers arise from the fact that the distributions in the west tend to be top heavy (dominated by cirrus), while in the east the distributions are more bottom heavy (dominated by boundary layer clouds). As noted above, the layers that populate these types have little to do with actual hydrometeor layers in the middle P_{top} regime. In the west, cirrus over boundary layer clouds conspire to produce $680 < P_{\text{top}} < 440$ hPa, while in the east erroneously placing layer tops near the inversion top artificially enhances the occurrence frequency in the middle types.

Considering the low cloud types, the Stratocumulus type appears in nearly all respects to be drawn from a common populations of geometrical properties. Of the three low types, Stratocumulus has the least amount of overlying high cloud in the west. The higher occurrence of high clouds co-occurring with lower-level clouds in the west are the predominant cause of rejecting the null hypothesis for the Cumulus and Stratus types between the two study regions.

6. Summary and conclusions

As a radiative quantity, P_{top} is a function of the vertical distribution of condensate throughout an atmospheric column as well as the thermodynamic properties of a column. It has been understood that the vertical distributions of clouds within the ISCCP P_{top}–τ types do not necessarily correspond to the cloud types that these bins are often taken to represent (Rossow and Schiffer 1999). However, the vertical distributions of actual hydrometeor layers within the ISCCP P_{top}–τ bins have not been well documented. We have conducted such an exercise here by simulating ISCCP P_{top} using a component of the ISCCP simulator known as ICARUS and using retrieved τ along the tracks of *CloudSat* and *CALIPSO*.

Chen and Del Genio (2009) note that ''ISCCP CTP-TAU histograms are neither what they were intended to be (a distribution of highest cloud-top heights) nor what they are sometimes mistaken to be (an actual vertical distribution of clouds), but are instead a hybrid of both.'' We find that to be true to varying degrees in the eastern and western Pacific study regions. While the upper troposphere ISCCP types are characterized primarily by hydrometeor layers in the upper troposphere, the Cirrostratus P_{top}–τ type is often populated by geometrically thin cirrus overlying reflective lower-level clouds. Such combinations of layers can be diagnosed as optically thick cirrus with ISCCP-like retrieval algorithms. It also seems clear that all cirrus are by no means contained within the high P_{top}–τ bins. As measured by *CloudSat* and *CALIPSO*, hydrometeor layers in the upper troposphere remain a significant component of the vertical distribution of clouds in every P_{top}–τ bin in the west Pacific study region with the exception of the Stratocumulus type. In the eastern study region, low-level layers are a predominant feature of every P_{top}–τ bin with the exception of Cirrus. In other words, the predominant cloud types in each region, cirrus in the west and boundary layer clouds in the east, are significant contributors to the radiatively defined characterizations of ISCCP statistics in eight of the nine common P_{top}–τ types. The P_{top}–τ ISCCP types are mixtures of various cloud genre, whose radiative properties conspire to produce similar TOA radiative signatures. Simply stated, we find that the use of passive radiometry to diagnose cloud geometrical properties should be considered valid only under idealized conditions where it is reasonably well known that a single hydrometeor layer of a single phase is the predominate climatological type.

Many studies examine the global radiative impact of clouds using cloud climatologies derived from passive radiometry (e.g., Hartmann et al. 2001; Raschke et al. 2005; Chen et al. 2000) or use such climatologies to

evaluate global models (e.g., Weare 2004; Zhang et al. 2005). An often unstated assumption in such studies is that the hydrometeor populations that occupy P_{top}–τ types in one region are in some respects statistically similar to the hydrometeor populations that occupy those types in other regions. We evaluate the validity of such assumptions using the observed distributions of hydrometeor layers collected by *CloudSat* and *CALIPSO* within P_{top}–τ ISCCP types using Kolmogorov–Smirnov similarity tests and find that among these two regions, Cirrostratus, Deep Convection, and Stratocumulus do appear to be drawn from similar geometrical populations of hydrometeor layers. In the remaining six of the nine ISCCP types, particularly those in the midtroposphere, this assumption of similarity is not valid. While the TOA radiative effects may be similar, the vertical distributions of radiative heating and surface cloud forcing can be expected to be significantly different for the Cirrus, Altocumulus, Altostratus, Nimbostratus, Cumulus, and Stratus ISCCP classifications.

The conclusions we draw from this study are only strictly relevant to the geometric properties of hydrometeor populations that occupy the nine ISCCP P_{top}–τ types in the regions and the time periods we have considered. Clearly, it is necessary to extend this evaluation globally. Also, these conclusions do not extend to the more sophisticated analyses of ISCCP diagnostics that use cluster analysis of P_{top}–τ statistics to define regimes (Tselioudis et al. 2013; Oreopoulos and Rossow 2011). These studies include additional information such as the total cloud cover fraction in constructing the cloud regimes, and it is likely that the hydrometeor populations that occupy the regimes would separate more significantly. Therefore, the next phase of this work will examine the extent to which the hydrometeor populations of these cloud regimes are statistically disjoint or not from one another.

Finally, our results address the fundamental limitations of passive remote sensing in evaluating the role of clouds in the climate system and, by contrast, illustrate the critical need for continuing the synergy of combined active and passive remote sensing of clouds from the space that has been realized with the A-Train (Stephens et al. 2008). Because of the broad continuum of hydrometeor layer properties that modulate the TOA radiative signatures and the limited ability of passive sensors alone to diagnose these properties (Stephens and Webster 1984; L'Ecuyer et al. 2006; Cooper et al. 2006), we find that passive sensors operating in isolation often provide statistically ambiguous descriptions of cloud properties. Furthermore, with cloud feedback continuing to be the fundamental source of uncertainty in accurately predicting climate change (Dufresne and Bony 2008), active remote sensing of clouds from space should be given high priority and expanded in scope instead of being delayed into the latter years of the next decade (NASA 2010).

Acknowledgments. This work benefited from the expertise of Sally Benson in porting the ISCCP simulator algorithm from Fortran to IDL. Stephanie Avey (while very pregnant) and Sally Benson implemented the analysis code in an operational environment. Dr. Steve Cooper provided his implementation of the Radiant model. Qiuqing Zhang helped in creating several of the cloud occurrence figures. This work benefitted greatly from significant and valuable critical comments provided by Dr. George Tselioudis during several revisions of the manuscript. Support was provided by NASA Jet Propulsion Laboratory (Award 1228646) and NASA Grants NNX07AT45G and NNX10AM42G.

REFERENCES

Ackerman, T. P., and G. M. Stokes, 2003: The Atmospheric Radiation Measurement Program. *Phys. Today,* **56,** 38–45.

Chen, T., W. B. Rossow, and Y. Zhang, 2000: Radiative effects of cloud-type variations. *J. Climate,* **13,** 264–286.

Chen, Y., and A. D. Del Genio, 2009: Evaluation of tropical cloud regimes in observations and a general circulation model. *Climate Dyn.,* **32,** 355–369, doi:10.1007/s00382-008-0386-6.

Christi, M. J., and P. Gabriel, 2004: Radiant 2.0: A user's guide. Paper 742, Department of Atmospheric Science, Colorado State University, 39 pp.

Cooper, S. J., T. S. L'Ecuyer, P. Gabriel, A. J. Baran, and G. L. Stephens, 2006: Objective assessment of the information content of visible and infrared measurements for cloud microphysical property retrievals over the global oceans. Part II: Ice clouds. *J. Appl. Meteor. Climatol.,* **45,** 42–62.

Dufresne, J.-L., and S. Bony, 2008: An assessment of the primary sources of spread of global warming estimates from coupled atmosphere–ocean models. *J. Climate,* **21,** 5135–5144.

Hartmann, D. L., L. A. Moy, and Q. Fu, 2001: Tropical convection and the energy balance at the top of the atmosphere. *J. Climate,* **14,** 4495–4511.

Howard, L., 1804: *On the Modification of Clouds.* J. Taylor, 4 pp.

Jakob, C., and G. Tselioudis, 2003: Objective identification of cloud regimes in the tropical western Pacific. *Geophys. Res. Lett.,* **30,** 2082, doi:10.1029/2003GL018367.

——, and C. Schumacher, 2008: Precipitation and latent heating characteristics of the major tropical western Pacific cloud regimes. *J. Climate,* **21,** 4348–4365.

——, G. Tselioudis, and T. Hume, 2005: The radiative, cloud, and thermodynamics properties of the major tropical western Pacific cloud regimes. *J. Climate,* **18,** 1203–1221.

Klein, S. A., and C. Jakob, 1999: Validation and sensitivities of frontal clouds simulated by the ECMWF model. *Mon. Wea. Rev.,* **127,** 2514–2533.

L'Ecuyer, T. S., P. Gabriel, K. Leesman, S. J. Cooper, and G. L. Stephens, 2006: Objective assessment of the information content of visible and infrared measurements for cloud

microphysical property retrievals over the global oceans. Part I: Liquid clouds. *J. Appl. Meteor. Climatol.,* **45,** 20–41.

Lopes, R. H. C., I. Reid, and P. R. Hobson, 2007: The two-dimensional Kolmogorov-Smirnov test. *Proc. XI Int. Workshop on Advanced Computing and Analysis Techniques in Physics Research,* Amsterdam, Netherlands, Nikhef, 12 pp. [Available online at http://v-scheiner.brunel.ac.uk/bitstream/2438/1166/1/acat2007.pdf.]

Mace, G. G., 2010: Cloud properties and radiative forcing over the maritime storm tracks of the Southern Ocean and North Atlantic derived from A-Train. *J. Geophys. Res.,* **115,** D10201, doi:10.1029/2009JD012517.

——, Q. Zhang, M. Vaughn, R. Marchand, G. Stephens, C. Trepte, and D. Winker, 2009: A description of hydrometeor layer occurrence statistics derived from the first year of merged *Cloudsat* and *CALIPSO* data. *J. Geophys. Res.,* **114,** D00A26, doi:10.1029/2007JD009755.

——, S. Houser, S. Benson, S. A. Klein, and Q. Min, 2011: Critical evaluation of the ISCCP simulator using ground-based remote sensing data. *J. Climate,* **24,** 1598–1612.

Marchand, R. T., G. G. Mace, and T. P. Ackerman, 2008: Hydrometeor detection using *CloudSat*—An Earth-orbiting 94-GHz cloud radar. *J. Atmos. Oceanic Technol.,* **25,** 531–546.

NASA, 2010: Responding to the challenge of climate and environmental change: NASA's plan for a climate-centric architecture for Earth observations and applications from space. NASA Rep., 48 pp. [Available online at http://science.nasa.gov/media/medialibrary/2010/07/01/Climate_Architecture_Final.pdf.]

Oreopoulos, L., and W. B. Rossow, 2011: The cloud radiative effect of International Satellite Cloud Climatology Project weather states. *J. Geophys. Res.,* **116,** D12202, doi:10.1029/2010JD015472.

Peacock, J. A., 1983: Two-dimensional goodness-of-fit testing in astronomy. *Mon. Not. Roy. Astron. Soc.,* **202,** 615–627.

Platnick, S., M. D. King, S. A. Ackerman, W. P. Menzel, B. A. Baum, J. C. Riedi, and R. A. Frey, 2003: The MODIS cloud products: Algorithms and examples from Terra. *IEEE Trans. Geosci. Remote Sens.,* **41,** 459–473.

Press, W. H., S. A. Teukolsky, W. T. Vetterling, and B. P. Flannery, 1992: *Numerical Recipes in Fortran 77: The Art of Scientific Computing.* 2nd ed. Cambridge University Press, 933 pp.

Raschke, E., A. Ohmura, W. B. Rossow, B. E. Carlson, Y.-C. Zhang, C. Stubenrauch, M. Kottek, and M. Wild, 2005: Cloud effects on the radiation budget based on ISCCP data (1991 to 1995). *Int. J. Climatol.,* **25,** 1103–1125.

Rossow, W. B., and T.-C. Zhang, 1995: Calculation of surface and top of atmosphere radiative fluxes from physical quantities based on ISCCP data sets: 2. Validation and first results. *J. Geophys. Res.,* **100** (D1), 1167–1197.

——, and R. A. Schiffer, 1999: Advances in understanding clouds from ISCCP. *Bull. Amer. Meteor. Soc.,* **80,** 2261–2287.

——, and Y. Zhang, 2010: Evaluation of a statistical model of cloud vertical structure using combined *CloudSat* and *CALIPSO* cloud layer profiles. *J. Climate,* **23,** 6641–6655.

——, ——, and J. Wang, 2005: A statistical model of cloud vertical structure based on reconciling cloud layer amounts from satellites and radiosonde humidity profiles. *J. Climate,* **18,** 3587–3606.

Sassen, K., and Z. Wang, 2008: Classifying clouds around the globe with the *CloudSat* radar: 1-year of results. *Geophys. Res. Lett.,* **35,** L04805, doi:10.1029/2007GL032591.

Schiffer, R. A., and W. B. Rossow, 1983: The International Satellite Clouds Climatology Project (ISCCP): The first project of the World Climate Research Programme. *Bull. Amer. Meteor. Soc.,* **64,** 779–784.

Schwartz, C., and G. G. Mace, 2010: Co-occurrence statistics of tropical tropopause layer cirrus with lower layers as derived from *CloudSat* and *CALIPSO* data. *J. Geophys. Res.,* **115,** D20215, doi:10.1029/2009JD012778.

Stephens, G. L., and P. J. Webster, 1984: Cloud decoupling of the surface and planetary radiative budgets. *J. Atmos. Sci.,* **41,** 681–685.

——, and Coauthors, 2008: *CloudSat* mission: Performance and early science after the first year of operation. *J. Geophys. Res.,* **113,** D00A18, doi:10.1029/2008JD009982.

Tselioudis, G., W. Rosow, Y. Zhang, and D. Konsta, 2013: Global weather states and their properties from passive and active satellite cloud retrievals. *J. Climate,* **26,** 7734–7746.

Wang, J., W. B. Rossow, and Y. Zhang, 2000: Cloud vertical structure and its variations from a 20-yr global rawinsonde dataset. *J. Climate,* **13,** 3041–3056.

Weare, B. C., 2004: A comparison of AMIP II model cloud layer properties with ISCCP D2 estimates. *Climate Dyn.,* **22,** 281–292, doi:10.1007/s00382-003-0374-9.

Webb, M., C. Senior, S. Bony, and J.-J. Morcrette, 2001: Combining ERBE and ISCCP data to assess clouds in the Hadley Centre, ECMWF and LMD atmospheric climate models. *Climate Dyn.,* **12,** 905–922.

Weisz, E., J. Li, W. P. Menzel, A. K. Heidinger, B. H. Kahn, and C.-Y. Liu, 2007: Comparison of AIRS, MODIS, *CloudSat* and *CALIPSO* cloud top height retrievals. *Geophys. Res. Lett.,* **34,** L17811, doi:10.1029/2007GL030676.

Williams, K. D., and G. Tselioudis, 2007: GCM intercomparison of global cloud regimes: Present-day evaluation and climate change response. *Climate Dyn.,* **29,** 231–250.

——, and M. J. Webb, 2009: A quantitative performance assessment of cloud regimes in climate models. *Climate Dyn.,* **33,** 141–157.

World Meteorological Organization, 1975: *International Cloud Atlas: Manual on the Observation of Clouds and Other Meteors.* Vol. I. World Meteorological Organization, 180 pp.

Zhang, M. H., and Coauthors, 2005: Comparing clouds and their seasonal variations in 10 atmospheric general circulation models with satellite measurements. *J. Geophys. Res.,* **110,** D15S02, doi:10.1029/2004JD005021.

Zhang, Y., S. Kein, G. G. Mace, and J. Boyle, 2007: Cluster analysis of tropical clouds using *CloudSat* data. *Geophys. Res. Lett.,* **34,** L12813, doi:10.1029/2007GL029336.